Adaptive Compliance Shaping with Human Impedance Estimation

by

Huang Huang

THESIS

Presented to the Faculty of the Graduate School of

The University of Texas at Austin

in Partial Fulfillment

of the Requirements

for the Degree of

Master of Science in Engineering

THE UNIVERSITY OF TEXAS AT AUSTIN

May 2020

Adaptive Compliance Shaping with Human Impedance Estimation

APPROVED BY

SUPERVISING COMMITTEE:

Luis Sentis, Supervisor

Farshid Alambeigi

Acknowledgments

I want to firstly acknowledge my supervisor, Dr. Luis Sentis, who has generously supported my study on the Adaptive Compliance Shaping and helped me with the purchase of the equipment. I also want to thank him for being supportive for my application to PhD study and encourage me to pursue advanced study. He also gave me so many useful advice for academia. He is generous about spending his time to meeting with me and discussing with me about my research. And he is patient with all the paper review processes with me. In addition, he cares about students' feelings and never hesitate to talk about that and offer help. Thank you Dr. Sentis for advising me for my master study. I am lucky to have you as my supervisor. Next I would like to acknowledge my master thesis committee member, Dr. Farshid Alambeigi. I enjoy taking his course of algorithm for sensor based robotics, which is a brilliant course and the materials are amazingly useful. He is such a good instructor. From the course, I can sense he is really an expert in his area and the way he gives the course is wonderful. He started with basic concepts and advanced gradually providing me not only the solid base but also the insightful deep view for this area.

During my two years study for my master degree, all the lab members in Human Center Robotics Lab are really nice to me and they are all my good friends. I would like to thank Binghan He, who gave me so many advice on my research and provided me insightful suggestions for my future. He taught me many things through the study about complex stiffness human model, which

is the first formal research I participated in this lab. He taught me how to propose a study problem, how can abnormal data inspire a research topic as well as how to plan my graduate study. He also helped me a lot for my first leading project about adaptive compliance shaping. Thank you Binghan He for being patient and mentor me through my research. I also want to thank Gray Tomas, who has always been patient for my questions and gave me great guidelines about coursework and research. He is generous to help me with my research and can always have insightful suggestions. Without him, my research and study would be so much more difficult. Thank you Gray Tomas for being both my friend and my teacher. I would like to thank Steven Jorgensen, who taught me about robotics and helped me with my thesis writing. He is patient to teach me about concepts and studies in robotics and he is generous to share his experience. Thank you Steven Jorgensen for being so helpful. I also want to thank Henry Cappel who cooperated with me for the research of adaptive compliance shaping. Thank you Henry Cappel. Without you I can't finish that research. In addition, I want to also thank Junhyeok Ahn, Minkyu Kim, and Jaemin Lee for providing me help with any problems I had. I want to thank Nicolas Brissonneau for being a good friend and organize so many fun events. I also want to thank Mihir Vedantam, Seung Hyeon Bang, Ryan Gupta, Gilbert Martinez and Jee-Eun Lee for being good friends and bring me out for fun. Without them, my life here would be so boring.

Next, I want thank Tiger, who accompanies me during my master study and provides me emotional support. Thank you for being with me and being such an angel to support me.

Finally, I want to thank my parents who have always been supportive

to me. Without their supports, I would never come here and have my master study.

Adaptive Compliance Shaping with Human Impedance Estimation

Huang Huang, M.S.E.
The University of Texas at Austin, 2020

Supervisor: Luis Sentis

Robotics has been a promising and popular research area for the past few decades. Among various applications of robotic, in many cases, human are involved in different manners. Therefore, as an important sub research area of robotics, human robot interaction has drawn decent attention recently. It has been deeply and widely studied. For human robot interaction, human play an important role. Undoubtedly, the more we know about human, the easier we can do human robot interaction and the better performance we can achieve in human robot interaction. One fascinating research topic of human robot interaction would be human in exoskeleton, where human play a key role in the mechanical design of exoskeleton as well as the control strategy design of exoskeleton.

Among all those applications, the augmentation exoskeleton is especially interesting due to its ability to amplify human. As mentioned previously, human properties are important for the design of exoskeleton. Unfortunately, despite many inspiring and deep studies about human properties and various proposed human models, human remains to be a complicated system

that is hard to predict and model. Furthermore, human is a dynamic system whose parameters keep changing with time, bringing more challenges. As we all know, limited understanding of the control plant will limit the performance of the controller and bring difficulties in the design of a controller. In fact, the performance of many existed controller for augmentation exoskeleton is limited by using conservative values of human property parameters. A straightforward way to solve this problem is to estimate human properties online. Under this circumstance, the main challenges are to develop a control strategy, whose performance can be exploited using the estimation of human properties and a reliable method to online estimate human properties. This thesis mainly presents an adaptive compliance shaping control strategy with human impedance estimation and a brief review of a newly proposed complex stiffness model of human.

Table of Contents

List of Tables

List of Figures

Chapter 1

Introduction

Robotic exoskeletons have been used for a range of applications including assistance with muscle impairment due to disease [19, 12, 34], control mechanisms for tele-operation robots [24, 5], and a means to augment the strength or increase the endurance of the human operator [48, 22, 37, 13].

Among all those applications, the augmentation exoskeleton has the ability to amplify human, which infers a promising future application in army, where the augmentation exoskeleton would help soldiers to lift equipment easier, saving their energy and making heavy equipment portable, in manufacturing, where workers can use augmentation exoskeletons to carry heavy package and components around, improving working efficiency, in architecture, where the builders can move building materials using augmentation exoskeletons.

The study on exoskeletons mainly focuses on the mechanical design and the controller design. The performance of the exoskeletons can be improved from multiple aspects. Some researchers improve the performance of exoskeletons through feedback control [19] or offline and online optimization of control parameters [37, 51]. Our study aims to improve the performance of a strength amplification exoskeleton—one that feedback couples exoskeleton joint torque to human joint torque in order to amplify human strength.

As we discussed earlier, human properties are the key points for the

controller design of the exoskeleton. Despite many inspiring and deep studies about human properties and various proposed human models, human remains to be a complicated system that is hard to predict and model. That is because the complexity of human. The biomedical model of human has not been fully understood and the human properties depend on many aspects, most of which are hard to measure. In addition, human is a dynamic system and the property parameters can vary with time with high frequency. Therefore, we have very limited information about human properties, bringing multiple challenges in this area. One great challenge, which is also the focus of this thesis, would be the control system design for human in exoskeleton. In the design of control systems involving humans interacting with exoskeletons, human properties such as dynamic stiffness, damping, and inertia determine the tuning of parameters in our controller, which therefore determine the performance and stability of the controller. To solve this problem, we need to choose a good model of human and find a way to estimate human model parameters to exploit the ability of our controller. This thesis presents an adaptive compliance shaping control strategy with human impedance estimation and a brief review of a newly proposed complex stiffness model of human.

In Chapter 2, we review some of the existing model of the humans and the newly proposed complex stiffness model of the human. There are different kinds of human models. Despite the varying in complexity and applications, perhaps the most well known model for the human joint is the second order mass spring damper model, where the human joint is modeled by a mass, a damper and a spring corresponding to human inertia, damping and stiffness. Researchers have discovered a linear relationship between human

stiffness and external torque [2, 8, 26]. There are also researches illustrating a linear relationship between the damping and the external torque [2, 26]. In addition, it is also found that there seems to be a constant damping ration among various subjects despite the inertia, damping and stiffness differences [22]. However, this nearly constant damping ratio is not well explained. A newly proposed complex stiffness model of the human [21] can explain this well and also suggests a relationship between the human damping and stiffness.

In Chapter 3, we talk about ways of estimating human model parameters and present our strategy for estimating human stiffness using hybrid sensors and a random forest model. The estimation of human properties has been studied for the past few decades and different methods have been proposed. Those methods can be roughly divided into two categories. The first consists on the estimation based on a physical model of human, where human properties can be fitted into a model with parameters pre-calculated empirically and with physical meanings. Thanks to the development of machine learning recently, human model estimation has benefited from the learning technology. The second category uses machine learning methods to estimate human properties based on the inputs from sensors. Those kinds of methods do not require a physical model of the human but are usually lack of physical meanings. In our study, we use a random forest model to estimate human stiffness which takes the inputs from surface electromyograph (sEMG) sensors and stretch sensors. This model does not require any foreknowledge about human model.

In Chapter 4, we present a compliance shaping method which benefits from our previously presented estimation method and we show simulation

results and experimental results for a subject interacting with a one degree of freedom single joint elbow joint exoskeleton, demonstrating the accuracy and validness of our method. The results include both the steady state response of the controller with a human interacting with the exoskeleton as well as the stability performance of this controller. We also compare the result with a robust controller to demonstrate a performance improvement.

1.1 Summary of Contributions

The main contribution of this study includes two parts. The first part is a stiffness estimation method based on data inputs from sEMG and stretch sensors. This method uses a random forest model to estimate human stiffness and is able to predict human stiffness with high accuracy. Compared with other studies, to our knowledge, our method has the highest accuracy. The second part is an adaptive compliance shaping control method which adapts controller parameter to the estimated stiffness online and the performance is proven to be better compared with a robust controller without stiffness estimation.

This thesis contains materials from [21] and [25]. In [21], my main contribution is the literature study, experiment conduction and data analysis. In [25], my main contribution is the literature study, problem statement, experiment design and conduction and data analysis.

Chapter 2

Human Joint Model

2.1 Summary

In this chapter, I introduce a commonly used human model, the mass spring damper model and a newly proposed human model, a complex stiffness model [21]. I introduce relationships between human properties including human inertia, stiffness and damping, and external torques and muscle contractions. I also briefly introduce the research background, experiment process and results, statistical data analysis and characteristics of the complex stiffness human model.

2.2 Contribution Statement

This chapter contains materials from [21]. My main contributions are on literature study, where I searched for similar studies and summarized experimental results addressing non zero phase shifts, experiment conduction, where I helped in designing the experiments, and data analysis, where I searched for statistical methods that can be used to prove the significance of the complex stiffness model.

2.3 Introduction

The stability of force amplification exoskeletons, like impedance controlled robots for physical human robot interaction, depends on the human impedance, and the exoskeleton must guarantee this coupled stability despite the variability in the human's behavior. Medically oriented studies often model the human as a spring, mass, damper system with time-varying parameters [8, 4]. For this model, many studies have suggested a linear relationship between human stiffness and external toques as well as that for human damping given external torques. However, in a recent study, this model is shown to be inaccurate. A more accurate model with a complex stiffness term is proposed in [21] based on experimental results. In addition, it is also found that there seems to be a constant damping ratio among various subjects despite inertia, damping and stiffness differences [22]. However, this nearly constant damping ratio is not well explained for the mass spring damper model. The newly proposed complex stiffness model of the human [21] can explain this well and also suggest a relationship between human damping and stiffness.

2.4 Mass Spring Damper Model for Human Joint

A well known and widely used model for human joint is the second order mass spring damper model as shown in the Figure 2.1. The dynamic equation of this model can be expressed as

$$F = m\ddot{x}^2 + b\dot{x} + k(x - x_0), \tag{2.1}$$

where for human, F is the external torque exerted on human, m is the inertia of human joint, b is the linear damping of human and k is the human joint

stiffness and x_0 is the spring origin position.

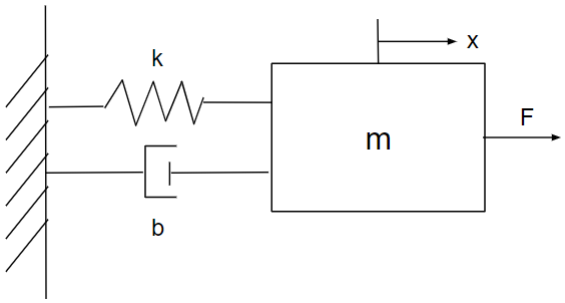

Figure 2.1: A mass spring damper system

In this spring, mass, damper model, several studies have revealed a linearity relationship between the human joint spring and the voluntary muscle contractions as well as the external torques exerted on the joint [4, 2, 8, 26]. In addition, it is also found that there exists a similar relationship between the damping and the muscle contractions and the external torque exerted on the joint [3, 50]. However, this linear relationship is statistically weaker than that for human stiffness [2, 26].

Since both the human stiffness and damping have linear relationship with the external torque and muscle contraction, it is instinctive to expect a relationship between human stiffness and damping. However, there is a lack of literature about the relationship between the human stiffness and the damping.

It has also been found that there is a near constant damping ratio for human joint despite the changing of human stiffness and human inertia [22]. A consistent damping ratio between 0.22 to 0.49 is shown through the frequency domain identification of the ankle joint [2, 16]. In addition, it is shown the damping ratio does not change significantly with the variation

of the external torque [50]. A multi-joint impedance study [44] on human arms also shows that for upper limbs, the damping ratio is distributed with a mean of 0.26 and a standard deviation of 0.08. Though multiple studies have pointed out this nearly constant ratio, it remains unclear why human has a constant damping ratio and the mass spring damper model fails to explain this phenomenon very well.

2.5 Complex Stiffness Model of Human

2.5.1 Introduction

As mentioned previously, the traditional mass spring damper model fails to explain the constant damping ratio. In addition, in some studies [8] (Fig. 6 of that paper), a non zero phase shift around 25 degrees in a wide range of low frequencies, in the phase plot of the bode plot of human joints are observed, which contradicts with the traditional mass spring damper model. This leads to the proposition of a new human joint model with complex stiffness [21], which consists of a hysteretic damping term and the human stiffness.

In biomechanical model, hysteretic damping models have seen success. There are experimental results [2] showing a hysteretic relationship between the applied torque and the ankle angle at very low frequencies. As mentioned before, there are non zero phase shifts observed which can be explained (in the field of structural mechanics) by defining a hysteretic damping whose damping coefficient is proportional to the inverse of frequency [6]. Hysteretic damping model have also been adapted to describe the dynamic properties of the whole body of a seated human [33] as well as cockroach legs [11].

In [21], the human stiffness and damping behavior for human in ex-

oskeleton are studied. Three models are compared: 1) a linear mass, spring, and viscous damper model, 2) a nonlinear complex-stiffness-spring and mass model (that is, a spring, mass, and hysteretic damper model), and 3) a combination model with mass, spring, and both viscous and hysteretic damping. And the significance of the hysteretic damping term is tested. Using a statistical method, F test, the statistical significance of the hysteretic damping term is shown. In addition, a linear relationship between this hysteretic damping term and stiffness is also studied which could explain the nearly constant damping ratio of human as well as the non zero phase shift observed both in previous studies [8] and the experiment results in this paper.

In [21], several experiments are conducted for a human wearing a one degree of freedom single joint elbow exoskeleton. During the experiments, the inertia of the exoskeleton are changed by attaching different loads at the end of the exoskeleton arm and the human stiffness are changed by applying different amount of external torques and asking the subject to squeeze an adjustable exercise hand grip. An augmentation controller is also used for some of the experiments. In [21], based on the newly proposed complex stiffness human model, a fractional order controller is also proposed which could make use of the non zero phase shift to achieve a more aggressive augmentation performance. The conceptual bode plot of this controller is shown in Figure 2.2 [21].

2.5.2 Experiment Results

In [21], the P0 series elastic elbow-joint exoskeleton from Apptronik Systems, as shown in Fig. 2.3 [21] is used to conduct the experiments.

In [21], an excitation chirp command (which essentially performs sys-

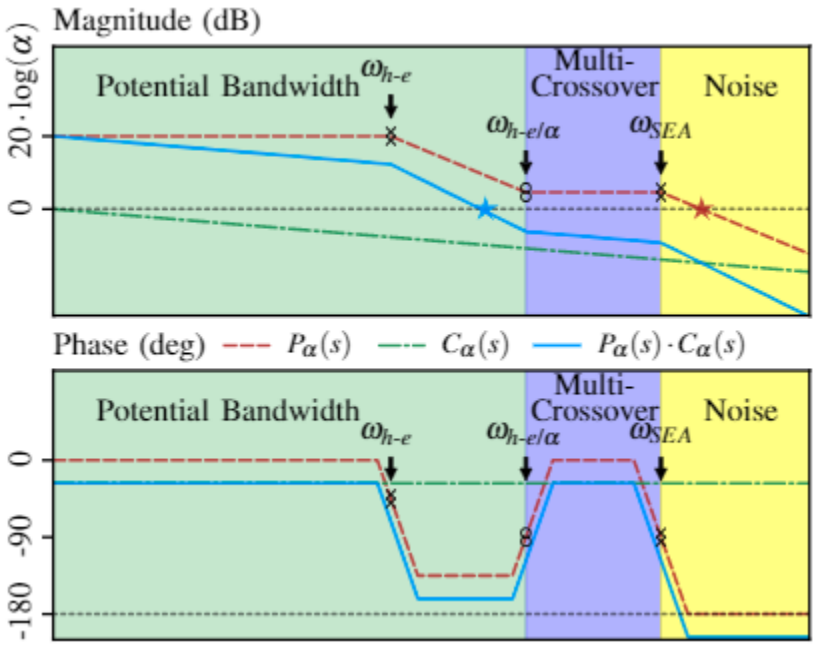

Figure 2.2: Conceptual bode plots show the augmentation plant $P_\alpha(s)$ with its poles (crosses) and zeros (circles). Regions are color-coded: the model is trustworthy in the green region, the blue region reflects the multi-crossover behavior which makes an augmentation controller design unreliable, and the yellow region is dominated by sensor noise from τ_c. A fractional-order filter $C_\alpha(s)$ brings $P_\alpha(s)$ to a lower crossover and increases the phase margin. The stars indicate the crossovers of $P_\alpha(s)$ and $P_\alpha(s)$ with $C_\alpha(s)$ [21].

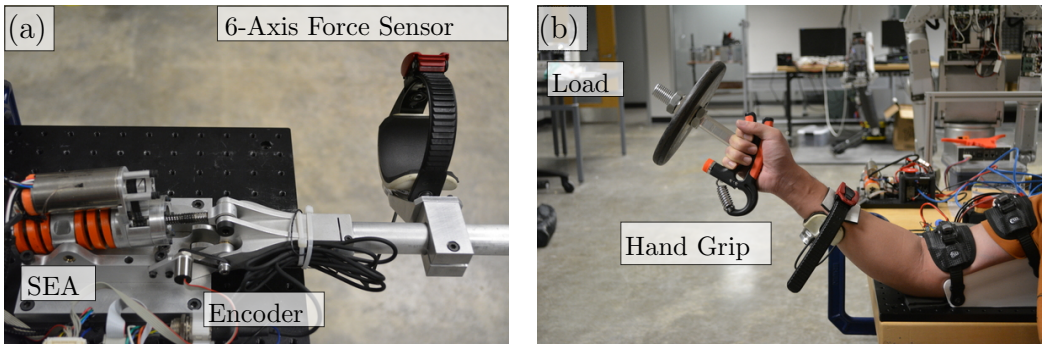

Figure 2.3: Experimental apparatus: a series elastic P0 exoskeleton from Apptronik Systems, featuring an ATI Mini40 force sensitive cuff and a P170 Orion air cooled series elastic actuator module acting through a simple 3 bar linkage [21].

Table 2.1: Experiment Parameters [21]

Exp	α	Load (kg)	Grip (kg)	Bias (Nm)	Amplitude (Nm)	Frequency (rad/s)
I.1	1	0.6				
I.2	1	2.3				
I.3	1	4.5	10	0	2α	$2-20$
I.4	2	4.5				
I.5	4	4.5				
II.1	1	0.6				
II.2	1	2.3				
II.3	1	4.5	14	4α	2α	$3-30$
II.4	2	4.5				
II.5	4	4.5				
III.1	1	0.6				
III.2	1	2.3				
III.3	1	4.5	27	8α	2α	$4-40$
III.4	2	4.5				
III.5	4	4.5				

tem identification of the human subject), a gravity compensation controller, a human augmentation controller, and a bias torque comprise the desired actuator torque signal. Three models described before can be expressed as $M1$, $M2$ and $M3$ as shown below [21].

$$S_{h\text{-}e/\alpha} = M_{h\text{-}e/\alpha}s^2 + B_h s + K_h, \tag{M1}$$

$$S_{h\text{-}e/\alpha} = M_{h\text{-}e/\alpha}s^2 + C_h j + K_h, \tag{M2}$$

$$S_{h\text{-}e/\alpha} = M_{h\text{-}e/\alpha}s^2 + B_h s + C_h j + K_h, \tag{M3}$$

where $M_{h\text{-}e/\alpha} = M_h + M_e/\alpha$ is the perceived inertia at the human joint,M_h is the inertia of human, M_e is the inertia of exoskeleton, α is the amplification ratio of the augmentation controller, B_h is the human damping, K_h is human stiffness and C_h is the hysteretic damping term.

In [21], the experiment parameter setting are shown in Table 2.1 [21]. α is the amplification ratio of the amplification controller, bias is the value of

the external torque and amplitude and frequency is that of the perturbation chirp command.

The experiment results fitted using $M3$ is shown in Figure 2.4 [21]. It easy to observe a non zero phase shift in the phase plot. And it is clear that the fitting is pretty good. And the parameter fitting results for all the three models are shown in Table 2.2 [21].

From Table 2.2, it is shown that there is a nearly constant damping ratio regardless human stiffness, inertia and the amplification ratio. Here the damping ratio for three models are defined as below [21]

$$\zeta_{h\text{-}e/\alpha} = \frac{B_h}{2\sqrt{K_h M_{h\text{-}e/\alpha}}} \qquad \text{for M1,} \tag{2.2}$$

$$\zeta_{h\text{-}e/\alpha} = \frac{C_h}{2K_h} = \frac{c_h}{2} + \frac{d_h}{2K_h} \qquad \text{for M2, and} \tag{2.3}$$

$$\zeta_{h\text{-}e/\alpha} = \frac{c_h}{2} + \frac{d_h}{2K_h} + \frac{B_h}{2\sqrt{K_h M_{h\text{-}e/\alpha}}} \qquad \text{for M3.} \tag{2.4}$$

In (2.3), $C_h = c_h K_h + d_h$ is the regression model between human stiffness and the hysteretic damping for $M2$. [21] reveals a linear relationship between human stiffness and the hysteretic damping for $M2$ and $M3$. The fitting results are shown below in Figure 2.5 [21]. The linearity between the hysteretic damping and the human stiffness is pretty significant and this relationship will help to reduce the parameter freedom in $M2$, making it easier to fit in practice. In addition, the non zero phase shifts at low frequencies shown in Figure 2.4 can be expressed as [21]

$$\text{Phase Shift} = \tan^{-1}(\frac{C_h}{K_h}) = \tan^{-1}(c_h + \frac{d_h}{K_h}) \text{ for M2, and} \tag{2.5}$$

$$\text{Phase Shift} = \tan^{-1}(c_h + \frac{d_h + B_h\omega}{K_h}) \qquad \text{for M3.} \tag{2.6}$$

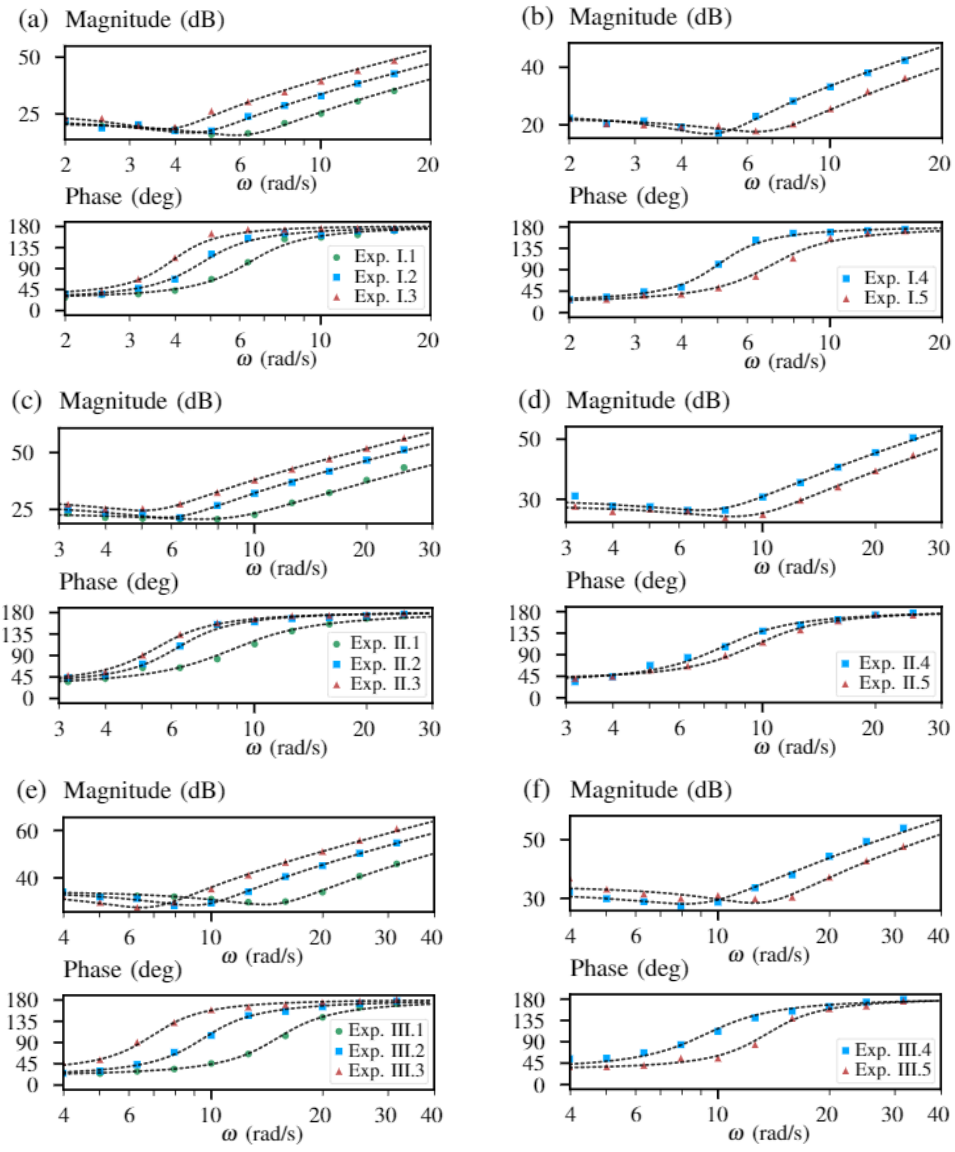

Figure 2.4: Bode plots of frequency domain data of $S_{h\text{-}e/\alpha}$ with Exp. I.1-5 on (a) and (b), Exp. II.1-5 on (c) and (d), and Exp. III.1-5 on (e) and (f). The dash lines on each plot show the fitted curves from M3 [21].

Table 2.2: Subject Dynamic Stiffness Parameters [21]

Exp	Model	$K_h(\frac{Nm}{rad})$	$C_h(\frac{Nm}{rad})$	$B_h(\frac{Nms}{rad})$	$M_{h\text{-}e/\alpha}(kgm^2)$	$\omega_{h\text{-}e/\alpha}(\frac{rad}{s})$	$\zeta_{h\text{-}e/\alpha}$
I.1	M1	10.05	--	1.03	0.28	5.95	0.31
	M2	10.05	5.89	--	0.28	5.95	0.29
	M3	10.05	4.97	0.18	0.28	5.95	0.30
I.2	M1	11.80	--	1.51	0.60	4.44	0.28
	M2	11.80	6.68	--	0.60	4.44	0.28
	M3	11.80	5.44	0.31	0.60	4.44	0.29
I.3	M1	15.74	--	2.09	1.18	3.65	0.24
	M2	15.74	8.33	--	1.18	3.65	0.26
	M3	15.74	10.44	−0.60	1.18	3.65	0.26
I.4	M1	13.82	--	1.46	0.60	4.78	0.25
	M2	13.82	6.87	--	0.60	4.78	0.25
	M3	13.82	6.01	0.21	0.60	4.78	0.25
I.5	M1	12.09	--	1.22	0.28	6.59	0.33
	M2	12.09	6.84	--	0.28	6.59	0.28
	M3	12.09	4.26	0.52	0.28	6.59	0.32
II.1	M1	12.73	--	1.41	0.20	7.94	0.44
	M2	12.73	10.18	--	0.20	7.94	0.40
	M3	12.73	5.86	0.66	0.20	7.94	0.44
II.2	M1	18.79	--	1.91	0.57	5.72	0.29
	M2	18.79	11.77	--	0.57	5.72	0.31
	M3	18.79	11.54	0.04	0.57	5.72	0.31
II.3	M1	25.95	--	3.08	1.03	5.02	0.30
	M2	25.95	16.75	--	1.03	5.02	0.32
	M3	25.95	15.48	0.26	1.03	5.02	0.32
II.4	M1	25.77	--	2.83	0.52	7.02	0.39
	M2	25.77	20.49	--	0.52	7.02	0.40
	M3	25.77	16.60	0.60	0.52	7.02	0.40
II.5	M1	19.07	--	1.88	0.28	8.32	0.41
	M2	19.07	16.27	--	0.28	8.32	0.43
	M3	19.07	15.72	0.08	0.28	8.32	0.43
III.1	M1	48.15	--	1.97	0.23	14.4	0.29
	M2	48.15	25.45	--	0.23	14.4	0.26
	M3	48.15	16.66	0.76	0.23	14.4	0.29
III.2	M1	48.60	--	2.85	0.58	9.13	0.27
	M2	48.60	25.61	--	0.58	9.13	0.26
	M3	48.60	15.19	1.23	0.58	9.13	0.27
III.3	M1	42.23	--	3.19	1.01	6.47	0.24
	M2	42.23	23.60	--	1.01	6.47	0.28
	M3	42.23	24.08	−0.07	1.01	6.47	0.28
III.4	M1	32.22	--	2.82	0.46	8.35	0.37
	M2	32.22	25.36	--	0.46	8.35	0.39
	M3	32.22	20.83	0.55	0.46	8.35	0.39
III.5	M1	42.33	--	2.08	0.27	12.43	0.31
	M2	42.33	26.50	--	0.27	12.43	0.31
	M3	42.33	27.66	−0.11	0.27	12.43	0.31

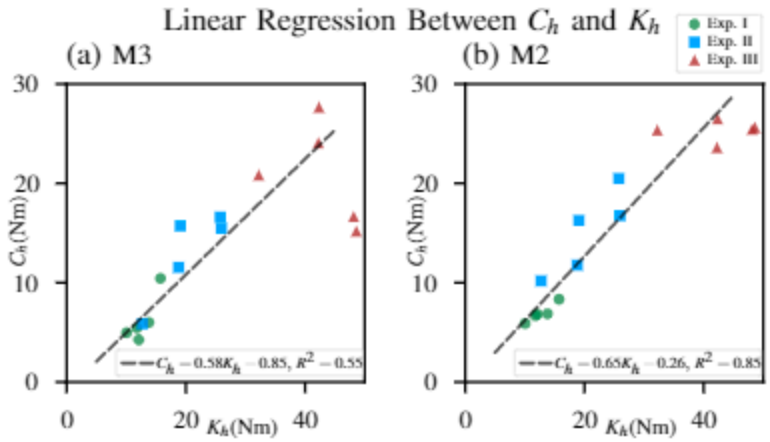

Figure 2.5: Linear regressions between C_h and K_h for M3 (a) and M2 (b) show that the parameters of M2 have a stronger linear relationship (that is, a higher R^2 value) [21].

2.5.3 Statistical Significance of the Hysteretic Damping Term

The statistical significance of the hysteretic damping term in $M2$ is calculated through F test [20]. F tests are conducted between $M1$ and $M3$ and $M2$ and $M3$ respectively. And the results of F tests for all experiments are shown in Figure 2.6 [21].

Figure 2.6 shows that for all experiments $M1$ is not significantly better than $M3$ but for 11 experiments out of 15 experiments, $M2$ is equally as good as $M3$. This shows that the hysteretic damping term has a significance impact on the accuracy of the model.

2.6 Conclusion

From [21], it is clear that a complex stiffness model is more accurate than the traditional mass spring damper model and therefore we use this model in our study of adaptive compliance shaping methods when conducting

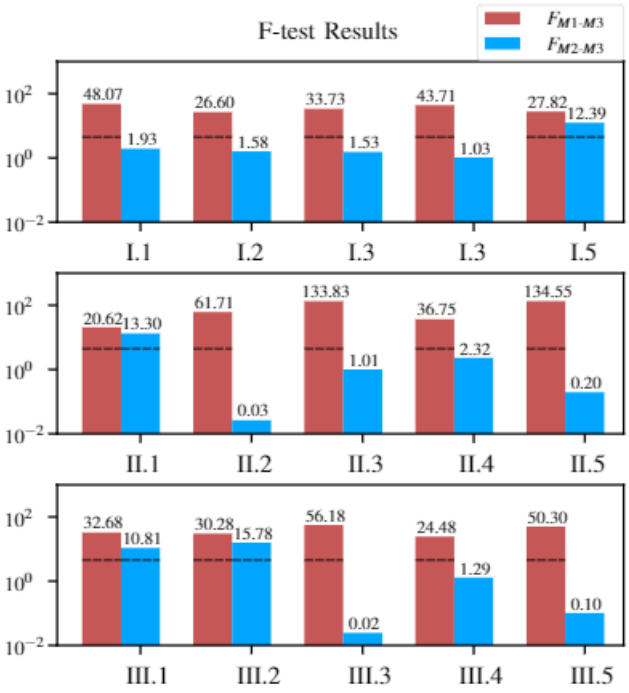

Figure 2.6: F-statistics on log scale for all experiments show the significant improvement on modeling accuracy from M1 to M3 and a partial improvement from M2 to M3. The dashed line appears on a bar if the F-statistic value is over the critical F-statistic value of 4.49 (false-rejection probability of 0.05) [21].

the simulation and designing the controller.

Chapter 3

Human Model Parameters Estimation

3.1 Summary

In this chapter, I introduce diffident methods of human properties estimation and the method I used in [25] to estimate human stiffness using a random forest predictor taking inputs from sEMG and stretch sensors. I introduce the experiment apparatus, protocol as well as the data processing and analysis methods. I also discuss the estimation results in detail.

3.2 Contribution Statement

This chapter contains materials from [25]. My main contributions are on the problem statement, where I proposed that sEMG sensors combined with stretch sensors can estimate human stiffness, the literature study, where I searched for similar studies and compared our methods and results, the experiment design, where I designed the experimental setting and process and built the hardware system, conducting the experiment where I collected and analyzed data and used different estimation models to chose the one with the most accuracy.

3.3 Introduction

There are different kinds of human estimation types which can be roughly divided into two categories. The first one is the estimation or prediction of human behaviors or human intention such as estimating human motion trajectories. For example, for assistive exoskeleton, the prediction of human intention can reduce time latency. For rehabilitation exoskeleton, the prediction of human intention facilitates physical movements. In addition, the prediction of human behavior is also an important toll for human robot interaction out of safety concerns or to better interact with humans.

Another category involving the use of human estimation and prediction is the estimation of human physical properties including human stiffness, damping and applied torque. This kind of estimation is also very useful in the design of exoskeletons. In assistive exoskeletons and rehabilitation systems, there are various studies on estimation of human applied torque which could reflect the human motion intention. In augmentation exoskeletons, the human applied torque sometimes is the input to the exoskeleton controller and therefore plays an important role in the control system design. However, in most cases, the estimation of human applied torque can be replaced with a contact force sensor which is more accurate and faster. For human stiffness and damping estimation, lots of studies have been done in the biomedical community where the estimation of stiffness can help with the treatment of certain type of diseases.

In the previous chapter, we talked about different human models including the traditional mass spring damper model and the newly proposed complex stiffness model. However, both of the models includes time varying parameters stiffness and damping which is hard to online identify. This

brings difficulties in the design of controller. Usually, in control community, the controller is designed on the most conservative range of human parameter values, which can provide very strong coupled stability guarantees [48, 1], however this wider space of possible human models restricts controller performance [30]. An estimate of human stiffness with lower uncertainty has the potential to improve bandwidth for both human-robot interaction controllers and amplification exoskeletons [48, 7, 49].

Exoskeletons can accomplish strength amplification through various control frameworks including adaptive control [9], admittance control[36], impedance control [28], loop-shaping design with a bounded human impedance [22], and by independently shaping the human and exoskeleton side compliance [48]. Ref. [22] emphasizes remaining robustly stable and used system identification with the human in the loop in order to obtain a robust model of a SISO "amplification plant". In this framework it is clear how widening the uncertainty restricts the choice of crossover point and closed loop bandwidth. The framework in [48] emphasizes what dynamics behaviors are possible with the exoskeleton by specifying behavior in terms of two dynamic compliance transfer functions (exo-side and human-side). This framing makes it easy to design the controller to avoid instability with different human stiffnesses. A physical spring in [48] guaranteed a minimum compliance for the spring and human system and was used to design the controller. But an online estimate of human stiffness could provide the same information, without softening the human's connection to the exoskeleton.

As mentioned previously, the estimation of stiffness could benefit many controller designs for augmentation exoskeleton. A common approach to measure human stiffness is to impose a perturbation torque and measure

deflection [41]. However, this method is only effective offline [32, 40, 46]. Online stiffness estimation methods include biological models [46, 14, 45] as well as artificial neural networks [32, 40], with only a subset of the estimation methods generalizing to multiple subjects [46, 45]. Most studies focusing on stiffness estimation use sEMG sensors [32, 40, 46, 14, 45], but physical deflection sensors may offer a less noisy means to gain information from the human [18]. In our study, we use an approach combining sEMG sensors with low cost stretch sensors (deflection-varying resistors) and using a random forest model to give the estimation results. Comparing our estimation results with other similar researches, our accuracy is shown to be the highest to our knowledge.

In this study we apply online estimation of human stiffness to adapt the force feedback gains of a strength amplification exoskeleton according to the estimated human stiffness. Our online human stiffness estimator uses a novel combination of sensors, and arguably improves over the state of the art for estimating the stiffness of the human elbow, boasting an R factor of 0.993 (c.f. 0.9266 in [32]), and a 17 Nm/rad max error (c.f. 30 Nm/rad in [40] and 80 Nm/rad in [46]).

3.4 Experiment Appratus

We propose an approach to estimate human stiffness online by using a trained random forest model taking advantage of signals from sEMG and stretch sensors as well as exoskeleton velocity and position.

We use a single degree of freedom elbow joint exoskeleton for this research. The P0 exoskeleton (Apptronik Systems Inc., Austin, TX), as shown in Figure 3.1, is a 3 bar linkage device powered by a series elastic

actuator (SEA) with a spring force tracking bandwidth of 10 Hz and reliable actuator torque conversion using a linkage table. The exoskeleton includes a 6-axis force torque sensor measuring the human exoskeleton contact forces. The human rests his or her upper arm on a white 3D printed mount beside the actuator. Exoskeleton position θ is measured by an encoder at the joint and contact torque τ_c is measured by the force torque sensor. The moment of inertia of the exoskeleton is 0.1 $\text{kg} \cdot \text{m}^2$ without any additional weight, but provides the option to include additional external weights. A laser pointer is attached to the end of the long bar to assist with precise position movement projecting onto a white board one meter in front of the subject wearing the exoskeleton. The white board contains three lines referring to initial position and upper and lower bounds of movement. A deviation around $\pm 3^\circ$ from those lines is acceptable.

In addition, we utilize 3 Myowear sEMG sensors (SparkFun Electronics, Niwot, CO) located on the upper arm and forearm (biceps brachii, triceps brachii, and brachioradialis muscles) of the subject and 2 stretch sensors (Images Scientific Instruments Inc., Staten Island, NY) attached around the middle of the forearm and upper arm connected to an Arduino Mega 2560 (SparkFun) by a breadboard. The sampling frequency for all sensors is 250 Hz. The full setup of the apparatus including the exoskeleton and the peripheral sensors are shown in Figure 3.1.

3.5 Experiment Protocol

The experimental protocol was approved by the Institutional Review Board (IRB) at the University of Texas at Austin. The IRB proposal is attached in the appendix. One healthy, male subject wore the 3 sEMG

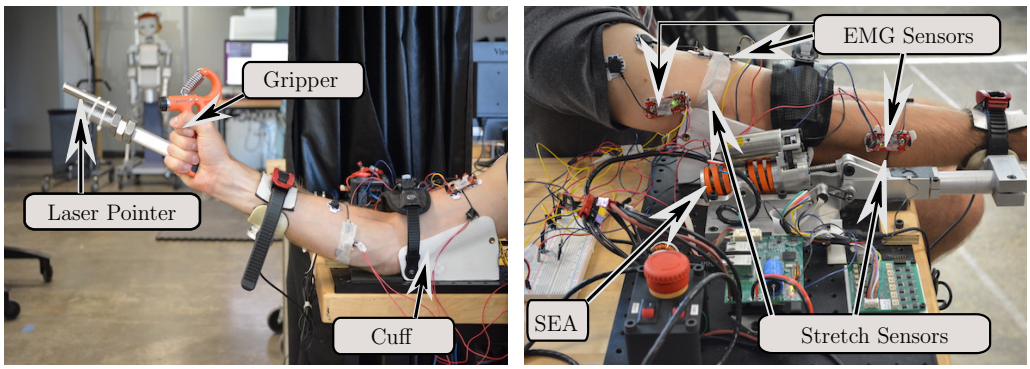

Figure 3.1: The P0 exoskeleton (Apptronik Systems Inc., Austin, TX) with an ATI Mini40 (ATI Industrial Automation, Apex, NC) force sensitive cuff located near the middle of the forearm. The subject holds a grip-strength exercise device to modulate co-contraction in the muscles at the elbow. The subject is instrumented with 3 sEMG sensors and 2 stretch sensors that are used to estimate stiffness [25].

sensors and 2 stretch sensors during the experiments.

The experiments are divided into 2 sections. The first consists of 11 experiments in which the participant maintains a constant equilibrium position while the exoskeleton imposes a torque comprising a piece-wise constant bias and a sinusoidal excitation with constant frequency and amplitude. In order to obtain reference signal values for all sensors, the participant initially holds a constant posture for 20 seconds, aligning the laser pointer to a target. The first 20 seconds includes gravity compensation, with no bias torque. Following this procedure, the exoskeleton induces bias forces ranging from 0 Nm to 9.5 Nm in 0.5 Nm steps occurring in 3 second intervals. Because we noticed there tends to be larger errors for the low bias torques, we repeated the first five bias forces twice. The participant is asked to maintain the same constant position and apply no voluntary compensation torque. Movement is induced by the sinusoidal signal, which has a constant frequency of 1 Hz

and amplitude of 1.5 Nm. This experiment is repeated 11 times (denoted I.1-11), with a 30 second resting period between every five bias force transitions as well as a minimum of 2 minutes resting period between each of the 11 experiments. In I.1, the subject holds nothing. To induce muscle co-contraction, I.2-11 introduce a hand-grip exercise tool with an adjustable load. The participant squeezes a gripper beginning with 22 lb for the second trial and up to 82 lb for the final trial.

The second set of experiments maintains the same procedure as the first experiment set except the participant voluntarily moves his or her arm at 0.5 Hz, using three optical targets for the midpoint and two extremes of the oscillation. In this experiment the sinusoidal excitation has a constant frequency of 1.7 Hz and an amplitude of 2.5 Nm. The bias force increases from 0 Nm to 8 Nm in step of 2 Nm occurring in 15 second intervals. All other parameters and procedures remain consistent with the first set of experiments (including the variation of grip strength). This set of experiments is denoted as II.1-11.

3.6 Estimation Methods

3.6.1 Data Preprocessing

In both experiment sections signals from 3 sEMG sensors are amplified, rectified, and integrated and then passed through a second order low pass filter with cutoff frequency of 60 rad/s and damping ratio of 0.707. We use the average signal values from 2 stretch sensors and 3 sEMG sensors in the first 20 seconds of each experiment as initial reference signal values for that experiment. These values are subtracted from the sEMG and stretch sensors' data to get the variation data for the 5 sensors. The absolute values

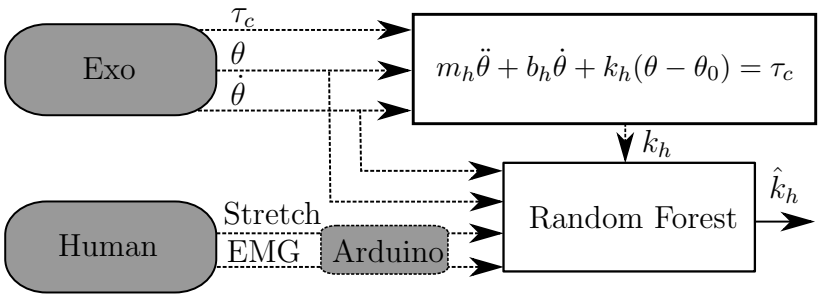

Figure 3.2: Diagram of training scheme for random forest predictor. Stiffness k_h is estimated using least squares fitting in the time domain, and is used as the ground truth for training the stiffness predicting random forest [25].

of processed data from the stretch and sEMG sensors are denoted as $S1$, $S2$ and $E1$, $E2$, $E3$ respectively.

In the first experiment section, exoskeleton position and velocity, and contact torque are filtered with the same second order low pass filter to calculate the reference stiffness.

In the second experiment section, we use a second order butterworth bandpass filter [27] with cutoff frequency of 1.2 Hz and 10 Hz for exoskeleton position and velocity, and contact torque to filter out the influence of human voluntary movement when calculating the reference stiffness.

For both sections, exoskeleton position and velocity are filtered by the same second order low pass filter to build the training and validation data set.

3.6.2 Time Domain Regression

In order to obtain a reference stiffness value for training the online estimation model and validating the accuracy, we use a linear regression for

the time domain data regarding the dynamic equation[1]

$$m_h\ddot{\theta} + b_h\dot{\theta} + k_h(\theta - \theta_0) = \tau_c \tag{3.1}$$

where τ_c is the contact torque between the human and exoskeleton, m_h, b_h, and k_h are the inertia, linear damping, and stiffness of the human, θ, $\dot{\theta}$ and $\ddot{\theta}$ are the joint position, velocity and acceleration of the human, and θ_0 is the equilibrium angle of the human spring (i.e. the human's desired position). In the case of a rigid connection between the human and exoskeleton, the human's joint position, velocity and acceleration are equal to the corresponding measurable properties of the exoskeleton. Through a linear regression between τ_c and $[\theta, \dot{\theta}, -1]$ for the corresponding experimental data ($\ddot{\theta}$ is not included due to the amplified noise from the double differentiation on joint position), we find the human stiffness k_h as the reference stiffness, linear damping b_h, and offset spring torque $\tau_0 = k_h\theta_0$. Each linear regression includes a moving window of 400 points in time.

3.6.3 Random Forest Predictor

Random forest is a learning method based on decision tree. It is wildly used for classification and regression problems. It trains multiple decision trees during the training process and averages the outputs of individual tree [23], correcting the over fitting problem of a single decision tree [15]. A random forest contains a large number of uncorrelated decision trees and each decision tree will make its own regression output using a standard supervised machine learning strategy. That means each tree will have

[1]Here, we use a linear damping model to estimate the human's stiffness, because of difficulties implementing hysteretic damping in the time domain regression. Hysteretic damping models are likely more accurate[21], and we use them for the stability analysis.

its individual error and their results have low correlation. By averaging all the regression outputs, the regression error is minimized and the over fitting problem is somewhat avoided. Compared with other machine learning technologies, random forest method has the advantage of high generality and less over fitting issue. Unlike convolutional neural network (CNN), whose performance is sensitive to the network structure, random forest method has a fixed structure and therefore is much easier to implement. In addition, it can also achieve relatively stable performance for different applications and therefore can be applied to more problems compared with CNN, which is widely used in computer vision,

We use a random forest predictor from scikit-learn package [43] in Python to estimate muscle stiffness based on a 7-dimensional training data set, which includes the absolute value of exoskeleton position and velocity, filtered by the second order low pass filter, and S1, S2, E1, E2 and E3. The reference stiffness values are used as a supervisory signal. The model is structured with an estimator number of 50 and a maximum depth of 10 for each estimator to avoid over-fitting. The predictor is trained offline with data from both the first and second experimental sections. The full diagram of the model training procedure is outlined in Fig. 3.2.

3.7 Results

We obtain 76350 offline shuffled data points where 50900 are used for offline training and the remaining 25450 are used as an offline validation set. The estimation results for all data sets using the trained random forest predictor give us a maximum error of 16.58 Nm/rad and an error variance of 2.55 Nm^2/rad^2. The results are shown in Fig. 3.3(a). Estimation results

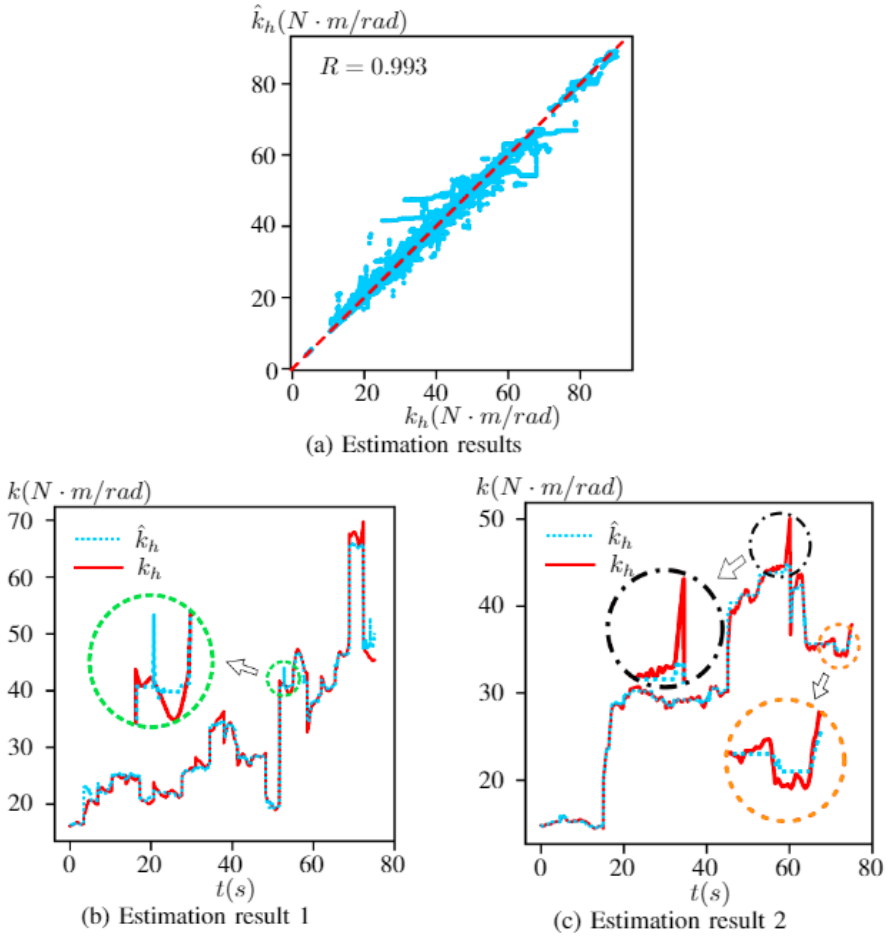

(a) Estimation results

(b) Estimation result 1

(c) Estimation result 2

Figure 3.3: Random forest predictor results. $\hat{k}_h$ is the estimated stiffness from our random forest predictor and k_h is the reference stiffness calculated from the time domain regression. Fig. 3.3(a) shows the linear relationship between the estimated stiffness and the reference stiffness for all experiments I.1-11 and II.1-11. The blue dots are the data points and the red dash line is the reference line of $y = x$. Fig. 3.3(b) shows estimation results from experiment group I. Fig. 3.3(c) shows estimation results from experiment group II [25].

for the validation data set only have a maximum error of 14.51 Nm/rad and an error variance of 3.01 Nm^2/rad^2. Representations of accurate estimation results are shown in Fig. 3.3(b) and Fig. 3.3(c) respectively.

The quality of our predictor is high relative to other published predictors of human stiffness using sEMG data. From Fig. 3.3(a) we notice a significant linear relationship between stiffness estimation and reference stiffness. Comparing the estimation results with other similar research, our R factor 0.993 points to a stronger correlation than the best result of elbow stiffness in [32] of 0.9266 ([32] uses an artificial neural network to estimate multi-joint stiffness, but we only compare the elbow joint stiffness results). Our stiffness ranges from 5 to more than 90 Nm/rad which is a more practical range compared with [32]'s smaller range of 1 to 3 Nm/rad. Our predictor has a maximum error less than 17 Nm/rad while Fig.5 in [40] shows a maximum error greater than 30 Nm/rad and the results in [46] show a maximum error greater than 80 Nm/rad. However, [46] uses a different definition of elbow stiffness and includes data for nine subjects, which may influence their estimation accuracy. In addition, all the experiments in [32, 40, 46, 45] are done without the human's voluntary movement, which weakens the validation of their models. Stiffness estimation in the presence of voluntary motion introduces new challenges, because these voluntary movements can be confused with the human's response to the perturbation. Our bandpass filter helps to remove the influence of human voluntary motion in the estimation procedure (the human's voluntary motion is below the lower cutoff frequency), but does not completely eliminate this influence. This implies that the reference human stiffness is not entirely trustworthy for the second experiment set.

The error between estimated stiffness and reference stiffness may come

from three sources: error caused by incorrect sensor data, error caused by the imperfect predictor, and error due to incorrect reference stiffness. The green circle of Fig. 3.3(b) demonstrates a sudden peak in the stiffness estimate, a peak which is not reflected in the smooth reference stiffness. This kind of instant peak may be caused by inaccurate sensor data corrupting the inputs to the stiffness predictor. An erroneous momentary sensor value may be due to buffer error or electrical noise, which will cause the predictor to return an incorrect estimation result. In Fig. 3.3(c), the error shown in the orange circle may be a pure inaccuracy from the predictor while the error in the black circle may be caused by the incorrect reference stiffness. Since k_h in Fig 3.3(c) is acquired using a band pass filter, this unusual sudden increase and decrease of reference stiffness in the black circle can be explained by human motion being abrupt enough to enter the bandpass region of the filter.

In general, our predictor gives an accurate stiffness estimation for both stiffness in isometric conditions and during voluntary movement. This random forest predictor can be used for online stiffness estimation. If we eliminate the data from the stretch sensors in the training data set, we notice a decrease of R factor from 0.993 to 0.987 and an increase of maximum error from 16.58 to 19.32 Nm/rad. The error variance also increases from 2.55 to 5.13 Nm^2/rad^2 validating the importance of including the data from the stretch sensors.

3.8 Conclusion

In this chapter, we present our stiffness estimation methods using a random forest model taking inputs from sEMG sensors and stretch sensors and compared the results with other similar research. It turned out that to

our knowledge, our method has the highest accuracy.

Chapter 4

Adaptive Compliance Shaping Control

4.1 Summary

In this chapter, I introduce control methods for augmentation exoskeletons and claim that some controllers can benefit from the estimation of human stiffness. I introduce the design of a compliance shaping controller which could benefit from the stiffness estimation process and develop a theoretical analysis. I introduce an experimental process and results to validate the performance improvement brought by the stiffness estimation process compared with a robust controller without stiffness estimation.

4.2 Contribution Statement

This chapter contains materials from [25]. My main contributions are on the problem statement, the literature study, where I searched for different augmentation controllers that could benefit from human stiffness estimation, simulation and analysis, where I did the simulation to tune the controller parameter and analyze the potential performance improvement brought by the stiffness estimation process, the experimental design and conduction of the experiments, where I designed the experimental process for both the adaptive and robust controllers to compare the performance, and on the data analysis, where I compared and discussed the results.

4.3 Introduction

Research has been done to incorporate human property estimates into controllers [17, 42, 29]. For example, the authors in [17] applied torque estimation to rehabilitation exoskeletons, the authors in [42] use joint angle estimation in a rehabilitation finger exoskeleton, and the authors in [17, 42] focus more on trajectory following and assistance. Most studies focus on the estimation of applied torque or human intention [28, 38, 10, 31]. In many cases this torque estimation is used as an alternative to contact force sensors between the human and exoskeleton. The researchers in [29] perform a dynamic stiffness estimation using a musculoskeletal model for a power assist exoskeleton, but focus on the reduction of vibrations due to EMG noise.

Various control strategies of exoskeletons have augmented the strength of the human by a significant factor. Methods used include a feedback controller [22], a compliance shaping controller [48], and admittance control [36]. All methods maximized amplification while remaining robustly stable, however were tuned to ensure stability based on conservative bounds of human stiffness estimation. The researchers in [48] incorporated a double compliance shaping method using series elastic actuators (SEAs) and a disturbance observer to mitigate nonlinear transmission effects. The controller increased the passivity of the device, but had the potential for higher bandwidth and amplification if an accurate online estimation of stiffness was possible. In [21], the fractional order controller proposed based on the complex stiffness model needs to be stable over the entire human stiffness range. Since human stiffness can vary from $2Nm/rad$ to $200Nm/rad$, the performance of the controller is highly limited. If we can integrate the stiffness estimation

method into this controller, we can expect a better performance.

In the previous chapter, we talked about different methods of human properties estimation and our method of estimating human stiffness. We also see that the controller performance is limited by the information about human stiffness. Although many studies have successfully estimated human impedance parameters, few have applied them to exoskeletons. In this study, we contribute a novel controller adaptation scheme (based on the compliance shaping framework [48]) that uses bounded-error stiffness information to improve bandwidth while remaining stable. This controller is then experimentally validated to A) remain stable as stiffness changes, B) lose stability when fed incorrect stiffness information, and C) improve strength amplification bandwidth relative to a robust control design.

4.4 Controller Adaptation Scheme

Since we have demonstrated that stiffness can be estimated online to a reasonable accuracy, we can now exploit this knowledge to design higher performance exoskeleton controllers.

The relationship between exoskeleton position and external torque can be expressed as

$$m_e s^2 \cdot \theta = \tau_e + \tau_c + \tau_s. \tag{4.1}$$

where τ_e is environment torque, τ_c is torque applied by the human, and τ_s is our control input. Exoskeleton inertia m_e includes the attached weight. We implement a compliance shaping amplification controller as $\tau_s = (\alpha(s) - 1)\tau_c$ so as to achieve the nominal behavior

$$m_e s^2 \cdot \theta = \tau_e + \alpha(s)\tau_c, \tag{4.2}$$

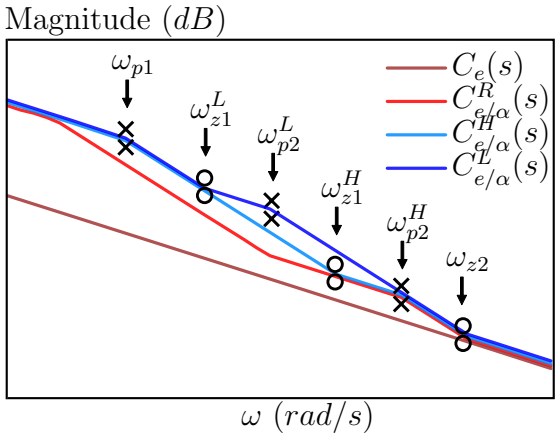

Figure 4.1: Conceptual bode plot shows the amplification performance for both the robust controller and the adaptive controller. $C_e(s)$ corresponds to the exoskeleton compliance. $C_{e/\alpha}^{H}(s)$ and $C_{e/\alpha}^{L}(s)$ correspond to the human side compliance of the exoskeleton using the adaptive controller when the human has a high stiffness and low stiffness. $C_{e/\alpha}^{R}(s)$ corresponds to the human side exoskeleton compliance using the robust controller [25].

where the human is amplified by a factor of $\alpha(s)$. This choice of control does not alter the environment-side compliance of the exoskeleton, $C_e(s) = 1/(m_e s^2)$. But it allows the human to feel an attenuated compliance $C_{e/\alpha}(s)$ of the exoskeleton as

$$C_{e/\alpha}(s) = \frac{\alpha(s)}{m_e s^2}, \tag{4.3}$$

which we refer to as the "human-side" compliance.

Our adaptation strategy determines a transfer function $\alpha(s)$ based on the measured human stiffness. We parameterize $\alpha(s)$ as

$$\alpha(s) = \frac{(s^2 + 2\zeta_0\omega_{z1}s + \omega_{z1}^2)(s^2 + 2\zeta_1\omega_{z2}s + \omega_{z2}^2)}{(s^2 + 2\zeta_0\omega_{p1}s + \omega_{p1}^2)(s^2 + 2\zeta_0\omega_{p2}s + \omega_{p2}^2)}. \tag{4.4}$$

The steady state amplification rate is $\alpha_{ss} = (\omega_{z1}^2\omega_{z2}^2)/(\omega_{p1}^2\omega_{p2}^2)$. The amplification $\alpha(s)$ approaches unity at high frequencies, making the torque feedback

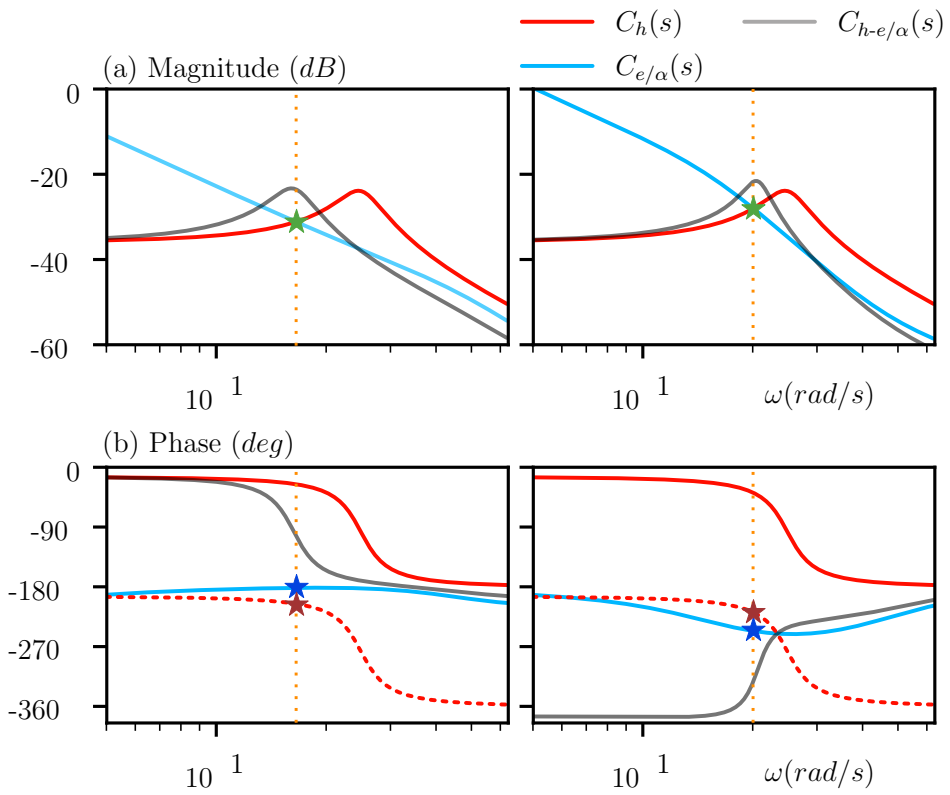

Figure 4.2: Bode plot showing stability behavior. The red dashed line in the phase plot is equal to $\phi(C_h(s)) - 180°$. The phase difference between the blue line and red dashed line determines the stability of the system. The left graph shows a stable system and corresponding phase behavior of the human in exoskeleton with conservative values of λ_1 and λ_2. The right graph shows an unstable behavior corresponding to more aggressive values of λ_1 and λ_2 [25].

$(1-\alpha(s))$ strictly causal, even though $\alpha(s)$ is not. For simplicity, we order the four natural frequency parameters $\omega_{p1},\ \omega_{z1},\ \omega_{p2},\ \omega_{z2}$ as shown in Fig. 4.1, and do not attempt to adapt the damping ratio ζ parameters. We place ω_{z2} at 10 Hz to avoid exceeding the bandwidth of the low level force controller, and this leaves us three free frequency parameters in the controller design. We remove one free parameter by fixing the desired steady state amplification ratio. As explained later, the gap between ω_{z1} and ω_{p2} must enclose a crossover frequency that depends on human stiffness. We constrain the remaining two degrees of freedom by choosing two tuning parameters λ_1 and λ_2 that ensure a sufficient distance between this crossover frequency and ω_{z1} and ω_{p2},

$$\lambda_1 = \frac{\omega_{h\text{-}e}}{\omega_{z1}}, \quad \lambda_2 = \frac{\omega_{p2}}{\omega_{h\text{-}e}}, \tag{4.5}$$

where $\omega_{h\text{-}e} = \sqrt{k_h/m_{h\text{-}e}}$ is the natural frequency of the human in the exoskeleton and $m_{h\text{-}e}$ is the inertia of the human and exoskeleton including the attached weight. The forearm inertia m_h has been measured for an average human at 0.1 kg m^2 in [8], but we do not know the inertia of our own subject.

Ultimately, we define our controller based on $\lambda_1,\ \lambda_2,\ \alpha_{ss}$ and the estimated value of $\hat{k}_h$:

$$\omega_{z1} = \frac{\omega_{h\text{-}e}}{\lambda_1} = \frac{1}{\lambda_1}\sqrt{\frac{\hat{k}_h}{m_{h\text{-}e}}}, \tag{4.6}$$

$$\omega_{p2} = \lambda_2\omega_{h\text{-}e} = \lambda_2\sqrt{\frac{\hat{k}_h}{m_{h\text{-}e}}}, \tag{4.7}$$

$$\omega_{p1} = \frac{\omega_{z1}\omega_{z2}}{\sqrt{\alpha_{ss}}\cdot\omega_{p2}}. \tag{4.8}$$

This allows us to change the shape of our amplification in real time. We refer to this real time compliance shaping controller as an adaptive controller in

this paper. In contrast, without real time stiffness estimation, we have to use the most conservative bound of human stiffness to calculate ω_{z1}, ω_{p1} and ω_{p2}, which reduces our amplification bandwidth, ω_{p1}. We refer to this as the robust controller.

The conceptual bode plot shown in Fig. 4.1 illustrates the improved performance using stiffness estimation and shows the amplification performance in different frequencies and values of stiffness. It is straightforward to find a better amplification performance of the compliance shaping controller with online stiffness estimation because the amount of uncertainty handled by the controller is reduced. The difference between the lines corresponding to $C^H_{e/\alpha}$ (the compliance shape when the human stiffness is high) and $C^L_{e/\alpha}$ (the shape when it is low) indicates the controller's shape changing with different stiffness values. In either case the steady state amplification behavior continues until ω_{p1}, a far higher bandwidth than that achieved by $C^R_{e/\alpha}$, the compliance shape that is robust to both human stiffness extremes.

The stability analysis for these controllers is based on the complex stiffness model of human impedance proposed in [21], with

$$C_h(s) = \frac{1}{m_h s^2 + k_h + c_h j}, \tag{4.9}$$

where c_h is the hysteretic damping of the human. According to [21],

$$\zeta_h = \frac{c_h}{2k_h}, \tag{4.10}$$

where ζ_h is the damping ratio of the human's elbow joint—which has been found to be nearly constant for repeated measurements of a subject [21, 39, 35]. We use a conservative, constant damping ratio of 0.13 to represent our subject. The parallel connection between human compliance and human side

exoskeleton compliance results in the total compliance of the human in the exoskeleton $C_{h\text{-}e/\alpha}(s)$ being a harmonic sum

$$C_{h\text{-}e/\alpha}(s) = \left(\frac{1}{C_h(s)} + \frac{1}{C_{e/\alpha}(s)} \right)^{-1}. \tag{4.11}$$

The stability of this system is determined by the phase margin of $\frac{C_{e/\alpha}(s)}{C_h(s)}$.

$$\frac{C_{e/\alpha}(s)}{C_h(s)} = \frac{\alpha(s)}{m_e s^2}(m_h s^2 + k_h + c_h j) \tag{4.12}$$

Therefore, the stability of this system can also be determined by the "human phase margin" of $C_{e/\alpha}(s)$,

$$\Delta\phi = \phi(C_{e/\alpha}(s)) - (\phi(C_h(s)) - 180^\circ). \tag{4.13}$$

The two bode plots in Fig. 4.2 show how large values of λ_1 and λ_2 produce a stable system (left) and how small values degrade the human phase margin and result in an unstable system (right). Note that the unstable system has a phase that rises rather than falling at the pole-pair—this indicates the poles are in the RHP.

As mentioned before, we do not know the inertia of our subject. Fortunately, in (4.13) reducing the phase of the human compliance increases the phase margin, and thus approximating human inertia as zero is conservative. We therefore choose values for λ_1 and λ_2 which guarantee stability for zero human inertia. In a more realistic test with human inertia based on [8], these parameters are confirmed to be stable.

4.5 Experiment Validation

We performed three tests to verify the stability, and bandwidth increase of the compliance shaping controller that incorporates the online stiff-

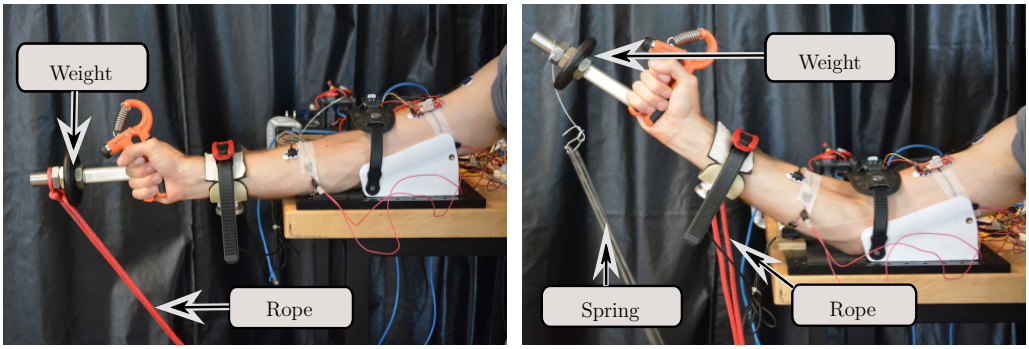

Figure 4.3: Experimental setup to verify the improvement of the controller. The left picture shows the setup of the bandwidth test and the right picture shows the setup of the stability test. The rope is in place to maintain a constant position in the bandwidth test and limit the range of position to protect the actuator in the stability test. In both tests, a 1.25 lb weight is attached to the end of the long bar (though this has no effect on the bandwidth test where the output is locked) [25].

ness estimation, as well as the significance of accurate online stiffness estimation.

4.5.1 Stability Test

We verify stability of the two controllers using a step response test. The experimental apparatus shown in the right image of Fig. 4 incorporates a spring attached to the end of the exoskeleton to induce an external force on the device. The removal of this spring acts as a step force excitation to the system.

The first experiment tests the robust controller. The participant wears the exoskeleton without the sEMG and stretch sensors and maintains a constant position while the spring is attached. After 10 seconds we remove the spring and observe the step response in the position signal. We repeat this procedure for a low stiffness (no gripper) and high stiffness case (the

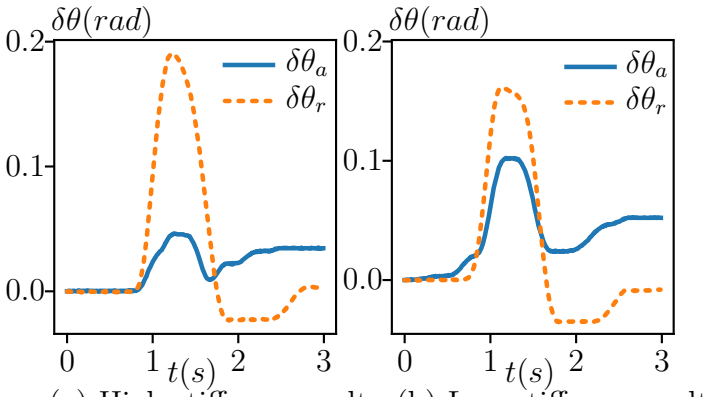

(a) High stiffness results (b) Low stiffness result

Figure 4.4: Stability test response shown by the exoskeleton position changing with time. $\delta\theta_a$ is the position change response of the adaptive controller and $\delta\theta_r$ is the robust controller response [25].

participant squeezes the gripper of 72 lb).

For the second experiment we repeat the same procedure, but using the adaptive controller. The participant wears the sEMG sensors on three muscle groups (biceps brachii, triceps brachii, and brachioradialis muscles) and stretch sensors positioned around the forearm and the midpoint of the biceps muscle on the upper arm to allow a real-time muscle stiffness estimate, which is also observed.

4.5.2 Bandwidth Increase Test

This experiment is designed to compare the bandwidth of the adaptive controller with the robust controller. The experimental setup shown in the left image of Fig. 4.3 incorporates a rope attached to the end of the exoskeleton to maintain a constant position by pulling against the hard-stop.

In order to verify the bandwidth improvement of the adaptive con-

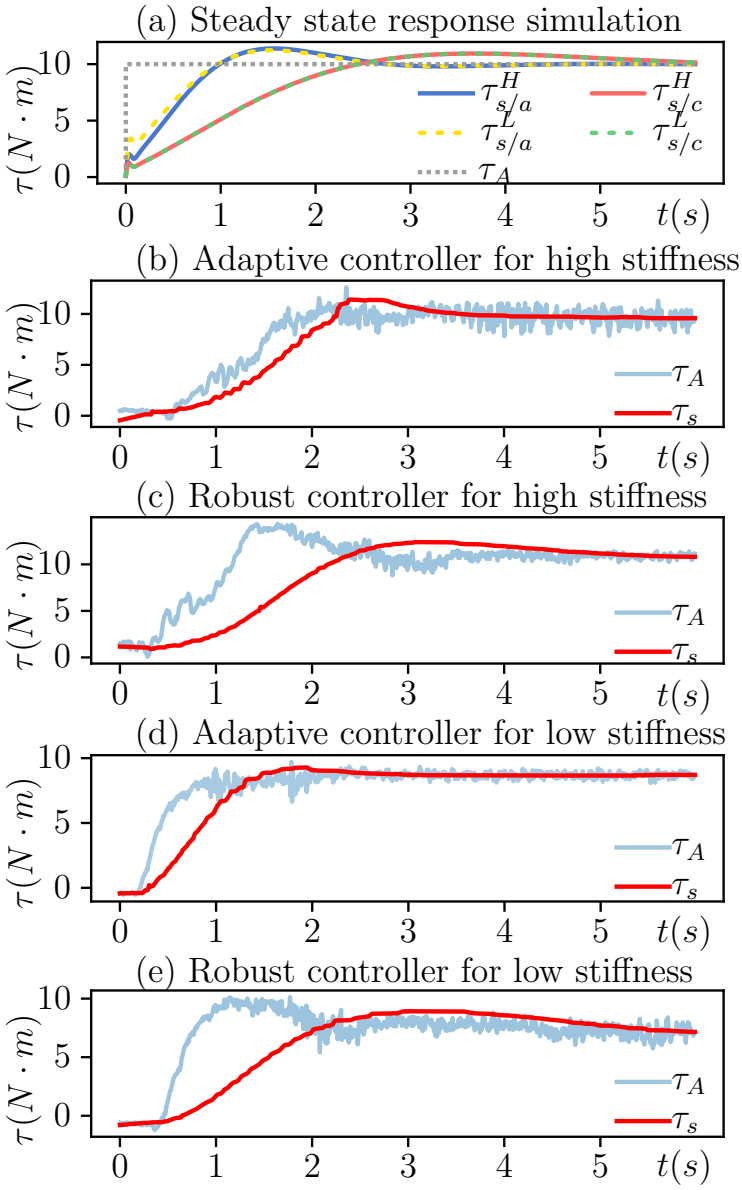

Figure 4.5: Steady state response for the bandwidth increase test. τ_s is the actuator torque. τ_A is equal to $-\alpha_{ss}\tau_c$ where τ_c is the contact force between the human and exoskeleton measured by the force sensor around the cuff. τ_A is the amplification torque we want to achieve. $\tau^H_{s/a}$ and $\tau^L_{s/a}$ are the simulated actuator torques of the adaptive controller in high stiffness and low stiffness. $\tau^H_{s/c}$ and $\tau^L_{s/c}$ are the simulated actuator torques of the robust controller in high stiffness and low stiffness [25].

troller, the participant wears the exoskeleton and generates a (near) constant force for 10 seconds. Actuator torque is observed. This process is repeated for the robust controller. For the purpose of maintaining a constant force during these trials a rope is attached to the end of the exoskeleton keeping the device in place.

4.5.3 Instability Test

The significance of accurate online stiffness estimation is measured by using the adaptive controller *without* real stiffness estimate data. Instead, a dummy stiffness estimate (60 Nm/rad) is used. In addition, the participant does not wear sEMG or stretch sensors. The setup is as the stability test, except that the step input is unnecessary. The subject maintains a constant position and relaxes their muscles for 10 seconds while the controller loses stability. After 10 seconds the participant maximally tenses their muscles and the controller regains stability.

4.5.4 Results

Results from these experiments are shown in Fig. 4.4, Fig. 4.5 and Fig. 4.6 respectively.

Fig. 4.4 shows that both controllers give a stable response to an impulse input, however the adaptive controller produces a smaller vibration amplitude than the robust controller for both cases of high stiffness and low stiffness. The lower overshoot amplitude of the adaptive controller response may be due to a better human phase margin and correspondingly better damping ratio in the human–robot system.

Fig. 4.5 shows both the simulation results of the steady state response

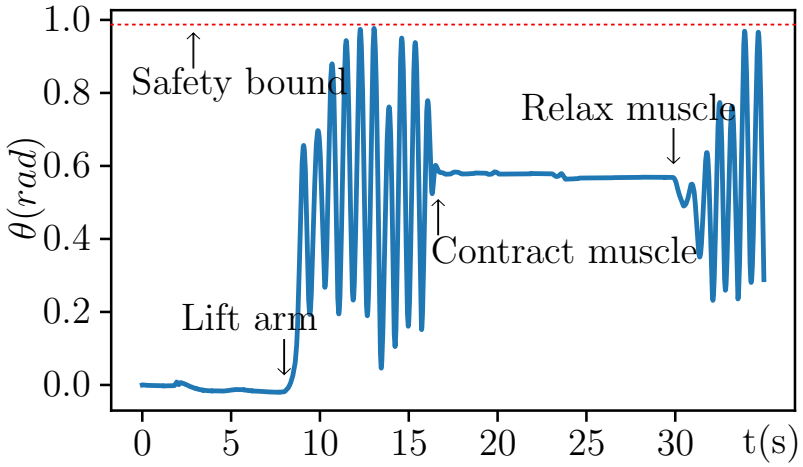

Figure 4.6: The instability test. The red dotted line at the top of the graph is the maximum position, as limited by the rope shown in the right picture of Fig. 4.3 [25].

with a step input (Fig. 4.5(a)) as well as experimental results (Fig. 4.5(b-e)). Fig. 4.5(b)(c) shows the comparison of the robust controller and the adaptive controller in the high stiffness case and Fig. 4.5(d)(e) shows the low stiffness case. The lag between τ_s and τ_A indicates the bandwidth of the controller. In both cases, the adaptive controller requires less time to achieve the target torque τ_A and therefore has a higher bandwidth. The experimental results appear consistent with the simulation results—large visual differences in the plots are largely due to the human input deviating from a perfect step.

Fig. 4.6 shows the instability test result. When the adaptive controller has a discrepancy between the estimated stiffness value and the actual stiffness value, the system becomes unstable as shown in Fig. 4.6. This experiment highlights the importance of accurate stiffness estimation to our adaptive controller.

4.6 Conclusion

In this chapter, we discussed that the online estimation of human stiffness could improve the performance of the controller. And we proposed a compliance shaping controller which could benefit from the stiffness estimation methods previously mentioned using a random forest model. We did both simulation and experiments to validate the performance improvement while maintaining stability.

Chapter 5

Conclusion and Discussion

In this chapter, I summarize the methods used in this study and discuss and compare the results. I also talk about limitations and future work.

5.1 Conclusion

Human impedance parameters play a key part in the stability of strength amplification exoskeletons. While many methods exist to estimate the stiffness of human muscles offline, online estimation has the potential to radically improve the performance of strength amplification controllers by reducing conservatism in the controller tuning. We propose an amplification controller with online-adapted exoskeleton compliance that takes advantage of a novel, online human stiffness estimator based on surface electromyography (sEMG) sensors and stretch sensors connected to the forearm and upper arm of the human. These sensor signals and exoskeleton position and velocity are fed into a random forest regression model that we train to predict human stiffness, with a training set that involves both movement and intentional muscle co-contraction. Ground truth stiffness is based on system identification in essentially perturburator-style experiments. Our estimator's accuracy is verified both by the offline validation results and by the stability of the controller even as stiffness changes (a scenario where the ground truth

stiffness is not available). Online estimation of stiffness is shown to improve the bandwidth of strength amplification while remaining robustly stable.

Many studies performed on amplification exoskeletons have relied on conservative bounds of human impedance properties [22, 7, 21]. Due to the difficulties of online estimation of human muscle stiffness [32, 40, 46, 45], few studies have attempted to improve amplification controller performance using these properties.

In this study, we propose an adaptive compliance shaping controller and demonstrate the improved performance due to stiffness estimation. The adaptive controller using the stiffness estimation provides increased stability and higher bandwidth than a comparable robust controller designed based on a conservative bound of human stiffness. We prove this improvement both theoretically and experimentally on a one DOF exoskeleton.

Accurate stiffness estimation is necessary to realize this compliance shaping controller. Our random forest predictor—using data from both sEMG and stretch sensors—was sufficiently accurate for this purpose. Our two experiment sections include training data from both isometric conditions and dynamic conditions with voluntary movement. Our estimation results appear to be more accurate than similar studies [32, 40].

5.2 Discussion and Future work

We use sEMG sensors and stretch sensors to estimate human stiffness. The estimation results may be further improved with better and more reliable sensors, as well as by taking into consideration the time delay of the filter. A higher accuracy would allow us to use a lower safety bound λ_1 and λ_2 to

achieve even higher bandwidth.

In this study, we only collected data from a single subject and trained a random forest model specified for this subject, which is non applicable to other subjects. In the future, we may include more subjects and train a more general random forest model applicable to multi subjects.

The convergence of the random forest predictor has not been proven, so it is difficult to make guarantees about the performance and safety of the predictor. As future work, we propose to integrate a backup safety controller [47] to take over if the learning system fails. Such a backup controller could offer firm safety guarantees, but would not interfere with the controller if it was not misbehaving.

The bandwidth increase test and the stability test point to performance improvement that can be realized with information about human properties. In this study, we use very conservative values of λ_1 and λ_2, calculated based on a zero human inertia assumption, for both the adaptive and robust controller, which limits the performance of both controllers. In future studies, we can use a more aggressive safety bound to achieve better performance for both controllers with accurate knowledge of human inertia. However, we can still expect the adaptive controller to outperform the robust controller. We believe this method can be applied to other kinds of controllers currently lacking knowledge of human impedance parameters. For instance the controllers in [22, 7, 21] may achieve similar bandwidth improvements with a similar system to update the human model online.

Appendix

Appendix 1

IRB proposal

1.1 Title

Online Determination of Muscle Stiffness to Improve the Performance of a Human Exoskeleton

1.2 Hypothesis

The integration of surface electromyography sensors, stretch sensors, piezoelectric sensors, or strain gauge sensors will help a robotic exoskeleton to estimate human muscle stiffness thus improving the overall performance of the device.

1.3 Study Background

The study will support one major goal consisting of multiple subgoals. The main goal of this study is to develop a method such that a human exoskeleton can better determine human muscle stiffness online and thus increase strength augmentation and stability of the controller. The main goal is divided into a series of subgoals each of which has the possibility for significant contribution in the robotics community. The first subgoal is to develop an accurate neural network structure to predict human stiffness based on data from position, velocity, torque sensors, surface electromyogra-

phy (sEMG) signals, piezoelectric sensors, strain gauge sensors, and stretch sensors. This will require training of the neural network and if an accurate and consistent structure is determined will lead to better performance of the exoskeleton. The training will require participants to maintain their arm or leg in the cuff while the exoskeleton performs a series of oscillatory motions. Data from the sensors will be collected, processed and used for training the network. The next subgoal is to test a dynamic model of stiffness based on torque, position, and velocity readings. Finally, the last subgoal leading to the overall structure of this project will be to run both methods in parallel and determine which method produces more accurate data which will then be used as input into the controller.

1.4 Design and Methodology

The study will consist of a series of tests of a participant wearing an arm or leg exoskeleton. The exoskeleton will impose a constant bias force on the participant and then a sinusoidal, impulse, chirp, or stochastic torque, which will move the participants leg or arm back and forth. Position, torque, velocity, surface electromyograph, piezoelectric, stretch, and strain gauge sensors will read information that will be recorded onto a data file. After training data has been collected the participant will test the effectiveness of the new controller by wearing the exoskeleton and moving their arm or leg back and forth.

1.5 Data Analysis

The researchers will be tracking encoder data that measures force and position values in the test bed's actuator. In addition the researchers will be collecting sEMG, strain gauge, piezoelectric, or stretch sensor data from electrodes attached to the participant's arm or leg. A subsection of the data will be used to train a neural network. The rest of the data will be used to verify the accuracy and efficiency of the neural network to determine human muscle stiffness. Finally, sensor data collected from testing the new controller will be analyzed to show the improvement of the controller.

1.6 Procedures

The researcher will brief the participant on the experiment and safety requirements, and will make sure that the participant has had any other questions answered. The safety requirements are very simple: (a) the user should keep their hands away from any pinch points in the actuator, (b) keep all body parts out of the way of the exoskeleton range of motion, and (c) the user should not touch any electronics (to protect the hardware - the electronics pose no real danger to the human). After this is done and the Informed Consent form is signed, the researcher will note basic, non-identifying information about the The researcher will brief the participant on the experiment and safety requirements, and will make sure that the participant has had any other questions answered. The safety requirements are very simple: (a) the user should keep their hands away from any pinch points in the actuator, (b) keep all body parts out of the way of the exoskeleton range of motion, and (c) the user should not touch any electronics (to protect the hardware - the electronics pose no real danger to the human). After this is done and

the Informed Consent form is signed, the researcher will note basic, non-identifying information about the participant under a generic name such as 'Subject 1'. The data here will be simple, such as the participant's height and weight. The researcher will check the participant's status throughout the test, ensuring at all times that they are not experiencing any issues.

The test itself will start by putting the participant's arm or ankle into an exoskeleton sensor cuff that is instrumented with an encoder, supported by an actuator, and capable of holding various weight loads from 0 to 25 lbs. The researcher will then place eight total sEMG electrodes, strain gauge sensors, piezoelectric sensors, or stretch sensors around the participant's arm or leg muscles. The participant will be asked to clench a gripper. The exoskeleton will impose a constant bias force and the participant will be asked to resist the exoskeleton to maintain their current position. The participant will be asked to relax their muscles to the best of their ability. The exoskeleton will then impose a sinusoidal, impulse, stochastic, or chirp torque which will move the participant's arm or leg back and forth well within their range of motion. After about 5 minutes, the exoskeleton will stop and the participant will be given 3 minutes to rest. After the resting period the participant will proceed through the exact same procedure except with a slightly different initial bias force. This process will be repeated ten times. After completing these, the participant will stop and take their arm/leg out of the cuff. After these tests the participant will put his or her arm or leg into the exoskeleton and move back and forth to test the improvement of the new controller. This test differs from the previous intervention in that the exoskeleton will not impose a defined torque to the participant, but instead the exoskeleton will only amplify the strength of the participant while the participant moves

at his or her own desire. The test will not input a significant amount of energy into the participants body. The torques imposed by the exoskeleton are moderate.

The experiments will take place in the Human Centered Robotics Laboratory (ASE 4.108) at the University of Texas at Austin. There will be 10 tests per day for 6 days, so the total time commitment will be no more than 560 minutes over 6 days. Participants can opt to have their photo taken for use in an academic paper. If they consent the researcher will take a photo of either their full body while wearing the exoskeleton or just their arm or leg in the exoskeleton.

1.7 Recruitment

Recruitment will be entirely on a volunteer basis, and it will mostly come from students on campus. They will be notified of the need for participants in the study via emails sent to various student groups that will then be passed on. We may also post fliers in the hallway requesting volunteers. A copy of the email is included with this application. The fliers will use the same or very similar wording as the attached email. We are not the instructors for any students who will participate.

1.8 Consent and Assent Processes

The researchers will obtain informed consent from the participant before proceeding to any other explanation of the experiment. The researchers will present the informed consent form to the participant and give them ample time to read through the document. Once the participant has read through

and signed giving consent, the researchers will proceed to give directions and begin the experiment.

1.9 Risks

This study is minimal risk. One risk to the participant is muscle fatigue after moving their arm or leg back and forth for many iterations during the experiment. Another risk is a breach of confidentiality of documents and/or data related to the participant. Lastly, there are pinch points on the exoskeleton and there is a risk of controller instability. The participant can stop the experiment at any point and all activities will cease. This will ensure that participants are not experiencing any muscle fatigue. The researcher will regularly ask the participant if they are feeling any fatigue. All data will be kept on a server that only researchers of this study will have access to. All consent forms will be kept in a locked cabinet in the Human Centered Robotic Lab that only researchers of this study will have access to. Pinch points will be outlined to the participants before the experiment commences to ensure they do not bring any body part near these areas. Finally, the researchers will impose torque limits on the actuators of the exoskeleton to ensure that if instability occurs the exoskeleton cannot move the participant's limb beyond a safe limit and the experiment will immediately cease.

1.10 Privacy

All experiments will take place in the Human Centered Robotics Laboratory away from the general public and students not working within the lab. If the participant is concerned with issues relating to privacy a curtain

can be used to shade the participant performing the experiment from all other students in the lab except the researchers. Basic readings such as the participant's weight or height will be kept on an MS Excel document saved to a lab server that only those approved research personnel in the Human Centered Robotics Lab will have access to. The encoder sensor readings collected during the experiments will be saved along with them, and for the sake of anonymity each participant's respective data will be labeled with generic names. Signed Informed Consent forms will be kept inside a locked cabinet in a lab with restricted access. All of these types of data will be kept for three years, after which time they will be deleted and shredded, respectively. As stated above, this time the Excel-sheet data will be anonymous, and will not be shared with other researchers for purposes not detailed in this study.

Bibliography

[1] Richard J Adams and Blake Hannaford. Stable haptic interaction with virtual environments. *IEEE Transactions on robotics and Automation*, 15(3):465–474, 1999.

[2] GC Agarwal and CL Gottlieb. Compliance of the human ankle joint. *Journal of Biomechanical Engineering*, 99(3):166–170, 1977.

[3] JD Becker and CD Mote. Identification of a frequency response model of joint rotation. *Journal of Biomechanical Engineering*, 112(1):1–8, 1990.

[4] DJ Bennett, JM Hollerbach, Y Xu, and IW Hunter. Time-varying stiffness of human elbow joint during cyclic voluntary movement. *Experimental Brain Research*, 88(2):433–442, 1992.

[5] Massimo Bergamasco, Benedetto Allotta, L Bosio, Luca Ferretti, G Parrini, GM Prisco, Fabio Salsedo, and G Sartini. An arm exoskeleton system for teleoperation and virtual environments applications. In *Proceedings of the 1994 IEEE International Conference on Robotics and Automation*, pages 1449–1454. IEEE, 1994.

[6] Richard Evelyn Donohue Bishop and Daniel Cowan Johnson. *The Mechanics of Vibration*. Cambridge University Press, 1960.

[7] S. P. Buerger and N. Hogan. Complementary stability and loop shaping for improved human robot interaction. *IEEE Transactions on Robotics*,

23(2):232–244, April 2007.

[8] Stephen C Cannon and George I Zahalak. The mechanical behavior of active human skeletal muscle in small oscillations. *Journal of Biomechanics*, 15(2):111–121, 1982.

[9] Shan Chen, Bin Yao, Zheng Chen, Xiaocong Zhu, and Shiqiang Zhu. Adaptive robust cascade force control of 1-dof joint exoskeleton for human performance augmentation. In *ASME 2015 Dynamic Systems and Control Conference*. American Society of Mechanical Engineers Digital Collection, 2016.

[10] C. Cheng, T. Huang, and H. Huang. Bayesian human intention estimator for exoskeleton system. In *2013 IEEE/ASME International Conference on Advanced Intelligent Mechatronics*, pages 465–470, July 2013.

[11] Daniel M Dudek and Robert J Full. Passive mechanical properties of legs from running insects. *Journal of Experimental Biology*, 209(8):1502–1515, 2006.

[12] Ryan J Farris, Hugo A Quintero, Spencer A Murray, Kevin H Ha, Clare Hartigan, and Michael Goldfarb. A preliminary assessment of legged mobility provided by a lower limb exoskeleton for persons with paraplegia. *IEEE Transactions on neural systems and rehabilitation engineering*, 22(3):482–490, 2013.

[13] Marco Fontana, Rocco Vertechy, Simone Marcheschi, Fabio Salsedo, and Massimo Bergamasco. The body extender: A full-body exoskeleton for

the transport and handling of heavy loads. *IEEE Robotics & Automation Magazine*, 21(4):34–44, 2014.

[14] David W Franklin, Frances Leung, Mitsuo Kawato, and Theodore E Milner. Estimation of multijoint limb stiffness from emg during reaching movements. In *IEEE EMBS Asian-Pacific Conference on Biomedical Engineering, 2003.*, pages 224–225. IEEE, 2003.

[15] Jerome Friedman, Trevor Hastie, and Robert Tibshirani. *The elements of statistical learning*, volume 1. Springer series in statistics New York, 2001.

[16] Gerald L Gottlieb and Gyan C Agarwal. Dependence of human ankle compliance on joint angle. *Journal of Biomechanics*, 11(4):177–181, 1978.

[17] K. Gui, H. Liu, and D. Zhang. A practical and adaptive method to achieve emg-based torque estimation for a robotic exoskeleton. *IEEE/ASME Transactions on Mechatronics*, 24(2):483–494, April 2019.

[18] Hyonyoung Han and Jung Kim. Active muscle stiffness sensor based on piezoelectric resonance for muscle contraction estimation. *Sensors and Actuators A: Physical*, 194:212–219, 2013.

[19] Omar Harib, Ayonga Hereid, Ayush Agrawal, Thomas Gurriet, Sylvain Finet, Guilhem Boeris, Alexis Duburcq, M Eva Mungai, Mattieu Masselin, Aaron D Ames, Koushil Sreenath, and Jessy W Grizzle. Feedback control of an exoskeleton for paraplegics: Toward robustly stable, hands-free dynamic walking. *IEEE Control Systems Magazine*, 38(6):61–87, 2018.

[20] Jeffrey F Harper. Peritz'f test: basic program of a robust multiple comparison test for statistical analysis of all differences among group means. *Computers in biology and medicine*, 14(4):437–445, 1984.

[21] B. He, H. Huang, G. C. Thomas, and L. Sentis. Complex stiffness model of physical human-robot interaction: Implications for control of performance augmentation exoskeletons. In *2019 IEEE/RSJ International Conference on Intelligent Robots and Systems (IROS)*, pages 6748–6755, 2019.

[22] Binghan He, Gray C Thomas, Nicholas Paine, and Luis Sentis. Modeling and loop shaping of single-joint amplification exoskeleton with contact sensing and series elastic actuation. In *2019 American Control Conference (ACC)*, pages 4580–4587. AACC, 2019.

[23] Tin Kam Ho. Random decision forests. In *Proceedings of 3rd international conference on document analysis and recognition*, volume 1, pages 278–282. IEEE, 1995.

[24] Bo Huang, Zhijun Li, Xinyu Wu, Arash Ajoudani, Antonio Bicchi, and Junqiang Liu. Coordination control of a dual-arm exoskeleton robot using human impedance transfer skills. *IEEE Transactions on Systems, Man, and Cybernetics: Systems*, 49(5):954–963, 2017.

[25] Huang Huang, Henry F. Cappel, Gray C. Thomas, Binghan He, and Luis Sentis. Adaptive compliance shaping with human impedance estimation, 2019.

[26] I.W. Hunter and R.E. Kearney. Dynamics of human ankle stiffness: Variation with mean ankle torque. *Journal of Biomechanics*, 15(10):747

– 752, 1982.

[27] Eric Jones, Travis Oliphant, and Pearu Peterson. Scipy: Open source scientific tools for python. 2001.

[28] Nikos Karavas, Arash Ajoudani, Nikos Tsagarakis, Jody Saglia, Antonio Bicchi, and Darwin Caldwell. Tele-impedance based assistive control for a compliant knee exoskeleton. *Robotics and Autonomous Systems*, 73:78–90, 2015.

[29] Toshihiro Kawase, Hiroyuki Kambara, and Yasuharu Koike. A power assist device based on joint equilibrium point estimation from emg signals. *Journal of Robotics and Mechatronics*, 24(1):205–218, 2012.

[30] Arvid QL Keemink, Herman van der Kooij, and Arno HA Stienen. Admittance control for physical human–robot interaction. *The International Journal of Robotics Research*, 37(11):1421–1444, 2018.

[31] K. Kiguchi and Y. Hayashi. An emg-based control for an upper-limb power-assist exoskeleton robot. *IEEE Transactions on Systems, Man, and Cybernetics, Part B (Cybernetics)*, 42(4):1064–1071, Aug 2012.

[32] Hyun K Kim, Byungduk Kang, Byungchan Kim, and Shinsuk Park. Estimation of multijoint stiffness using electromyogram and artificial neural network. *IEEE Transactions on Systems, Man, and Cybernetics-Part A: Systems and Humans*, 39(5):972–980, 2009.

[33] Satoshi Kitazaki and Michael J Griffin. Resonance behaviour of the seated human body and effects of posture. *Journal of Biomechanics*, 31(2):143 – 149, 1997.

[34] Hian Kai Kwa, Jerryll H Noorden, Matthew Missel, Travis Craig, Jerry E Pratt, and Peter D Neuhaus. Development of the ihmc mobility assist exoskeleton. In *2009 IEEE International Conference on Robotics and Automation*, pages 2556–2562. IEEE, 2009.

[35] F. Lacquaniti, F. Licata, and J. F. Soechting. The mechanical behavior of the human forearm in response to transient perturbations. *Biological Cybernetics*, 44(1):35–46, May 1982.

[36] Alexandre Lecours, Boris Mayer-St-Onge, and Clément Gosselin. Variable admittance control of a four-degree-of-freedom intelligent assist device. In *2012 IEEE International Conference on Robotics and Automation*, pages 3903–3908. IEEE, 2012.

[37] Sangjun Lee, Jinsoo Kim, Lauren Baker, Andrew Long, Nikos Karavas, Nicolas Menard, Ignacio Galiana, and Conor J Walsh. Autonomous multi-joint soft exosuit with augmentation-power-based control parameter tuning reduces energy cost of loaded walking. *Journal of neuroengineering and rehabilitation*, 15(1):66, 2018.

[38] Z. Li, B. Wang, F. Sun, C. Yang, Q. Xie, and W. Zhang. semg-based joint force control for an upper-limb power-assist exoskeleton robot. *IEEE Journal of Biomedical and Health Informatics*, 18(3):1043–1050, May 2014.

[39] T. E. Milner and Caroline Cloutier. Damping of the wrist joint during voluntary movement. *Experimental Brain Research*, 122(3):309–317, Sep 1998.

[40] Farid Mobasser and Keyvan Hashtrudi-Zaad. A method for online estimation of human arm dynamics. In *2006 International Conference of the IEEE Engineering in Medicine and Biology Society*, pages 2412–2416. IEEE, 2006.

[41] FA Mussa-Ivaldi, N Hogan, and E Bizzi. Neural, mechanical, and geometric factors subserving arm posture in humans. *Journal of Neuroscience*, 5(10):2732–2743, 1985.

[42] J. Ngeo, T. Tamei, T. Shibata, M. F. F. Orlando, L. Behera, A. Saxena, and A. Dutta. Control of an optimal finger exoskeleton based on continuous joint angle estimation from emg signals. In *2013 35th Annual International Conference of the IEEE Engineering in Medicine and Biology Society (EMBC)*, pages 338–341, July 2013.

[43] F. Pedregosa, G. Varoquaux, A. Gramfort, V. Michel, B. Thirion, O. Grisel, M. Blondel, P. Prettenhofer, R. Weiss, V. Dubourg, J. Vanderplas, A. Passos, D. Cournapeau, M. Brucher, M. Perrot, and E. Duchesnay. Scikit-learn: Machine learning in Python. *Journal of Machine Learning Research*, 12:2825–2830, 2011.

[44] Eric J Perreault, Robert F Kirsch, and Patrick E Crago. Multijoint dynamics and postural stability of the human arm. *Experimental Brain Research*, 157(4):507–517, 2004.

[45] Serge Pfeifer, Heike Vallery, Michael Hardegger, Robert Riener, and Eric J Perreault. Model-based estimation of knee stiffness. *IEEE Transactions on Biomedical Engineering*, 59(9):2604–2612, 2012.

[46] Duk Shin, Jaehyo Kim, and Yasuharu Koike. A myokinetic arm model for estimating joint torque and stiffness from emg signals during maintained posture. *Journal of neurophysiology*, 101(1):387–401, 2009.

[47] Gray C Thomas, Binghan He, and Luis Sentis. Safety control synthesis with input limits: a hybrid approach. In *2018 Annual American Control Conference (ACC)*, pages 792–797. IEEE, 2018.

[48] Gray Cortright Thomas, Jeremiah M Coholich, and Luis Sentis. Compliance shaping for control of strength amplification exoskeletons with elastic cuffs. *arXiv preprint arXiv:1903.09673*, 2019.

[49] Toru Tsumugiwa, Ryuichi Yokogawa, and Kei Hara. Variable impedance control based on estimation of human arm stiffness for human-robot cooperative calligraphic task. In *Proceedings 2002 IEEE International Conference on Robotics and Automation (Cat. No. 02CH37292)*, volume 1, pages 644–650. IEEE, 2002.

[50] PL Weiss, IW Hunter, and RE Kearney. Human ankle joint stiffness over the full range of muscle activation levels. *Journal of Biomechanics*, 21(7):539–544, 1988.

[51] Juanjuan Zhang, Pieter Fiers, Kirby A Witte, Rachel W Jackson, Katherine L Poggensee, Christopher G Atkeson, and Steven H Collins. Human-in-the-loop optimization of exoskeleton assistance during walking. *Science*, 356(6344):1280–1284, 2017.

Vita

Huang Huang received her B.S. in Engineering from Shanghai Jiao Tong University (SJTU) on June 2018. In 2018, she obtained Cockrell School of Engineering Fellowship at the University of Texas at Austin.

Permanent address: huangh at utexas.edu

This thesis was typeset with LaTeX by the author.